Transmission Torque Characteristics in a Magnetic Gear

Noboru Niguchi, Katsuhiro Hirata, Masari Muramatsu, and Yuichi Hayakawa

***Abstract* -- This paper describes the transmission torque characteristics in a surface permanent magnet-type (SPM-type) magnetic gear. The operating principle of this gear and its transmission torque under the synchronous operation in accordance with the gear ratio are formulated. And the high-order components contained in the cogging torque are verified by employing the 3-D finite element method (FEM) and carrying out measurements on a prototype. Furthermore, a method for reducing the cogging torque is discussed.**

***Index Terms*--3-D finite element method, cogging torque, magnetic gear, skew.**

I. Introduction

MAGNETIC gears have some advantages such as low mechanical loss and maintenance-free operation that are not observed in conventional mechanical gears. In addition, they operate as a torque limiter under overloaded condition, and magnetic gears are expected to be applied to a joint of the human robot. However, most of previous magnetic gears have a problem of insufficient transmission torque for practical use due to the narrow facing area between two rotors (Fig. 1).

Recently, various types of new magnetic gears to solve the above problem were proposed [1]-[5], and a SPM-type magnetic gear employing magnetic harmonics comes to attract attention because of its high transmission torque density though it has a complex structure with multipole magnets as shown in Fig. 2. Some studies on a SPM-type magnetic gear have been carried out, but few papers concerning the cogging torque can be seen.

This paper describes the transmission torque characteristics in a SPM-type magnetic gear. The operating principle and the transmission torque under the synchronous operation in accordance with the gear ratio are formulated [6]-[12]. High-order components contained in the cogging torque are computed by employing the 3-D FEM and the result of the analysis is verified by carrying out measurements on a prototype. Furthermore, a method for reducing the cogging torque is discussed.

II. Operating Principle

Assuming that a low-speed rotor is removed, only a high-speed rotor magnet generates magnetomotive force shown in Fig. 3(a), and stationary pole pieces generate permeance shown in Fig. 3(b), where θ represents rotor angle.

In this model, Fourier series expansions of $F(\theta)$ and $R(\theta)$ are shown in (1) and (2), respectively.

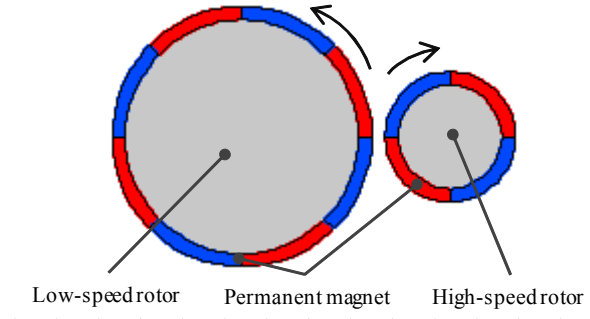

Fig. 1 Conventional magnetic gear.

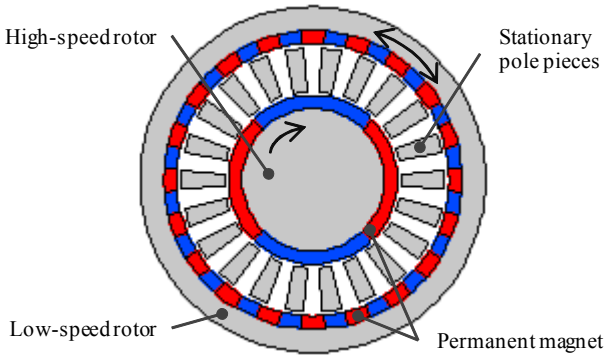

Fig. 2 SPM-type magnetic gear.

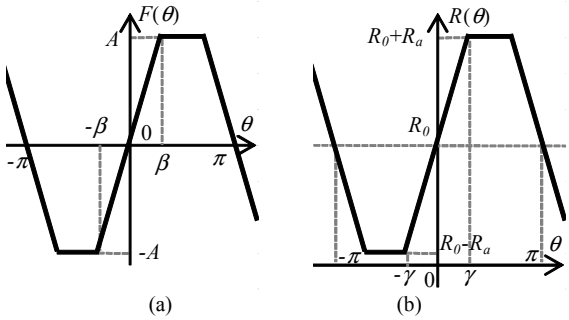

Fig. 3 Distributions of (a) magnetomotive force, and (b) permeance.

$$F(\theta)=\sum_{m=1}^{\infty}a_m\sin\{(2m-1)N_h\theta\} \tag{1}$$

$$R(\theta)=R_o+\sum_{l=1}^{\infty}a_l\sin\{(2l-1)N_s\theta\} \tag{2}$$

where N_h is the number of pole pairs in the high-speed rotor, N_s is the number of stationary pole pieces. And magnetic flux $\phi(\theta)$ can be obtained as follows:

$$\begin{aligned}\phi(\theta)=&\sum_{m=1}^{\infty}a_mR_0\sin\{(2m-1)N_h\theta\}\\&+\sum_{l=1}^{\infty}\sum_{m=1}^{\infty}a_la_m[\cos\{(2l-1)N_s-(2m-1)N_h\}\theta\\&-\cos\{(2l-1)N_s+(2m-1)N_h\}\theta]\end{aligned} \tag{3}$$

Magnetic flux contains $H_1(m)$, $H_2(l,m)$, and $H_3(l,m)$ orders shown in (4).

N. Niguchi, K. Hirata, M. Muramatsu, and Yuichi Hayakawa are with the Department of Adaptive Machine Systems, Graduate School of Engineering, Osaka University, Yamadaoka, Suita, Osaka, 565-0871 Japan (e-mail:noboru.niguchi@ams.eng.osaka-u.ac.jp).

978-1-4244-4175-4/10/$25.00 ©2010 IEEE

$$\begin{cases} H_1(m) = (2m-1)N_h \\ H_2(l,m) = (2l-1)N_s - (2m-1)N_h \\ H_3(l,m) = (2l-1)N_s + (2m-1)N_h \end{cases} \quad (4)$$

A high-speed rotor is rotated with $\Delta\theta$, then magnetic flux $\phi(\theta)$ can be derived as follows:

$$\phi(\theta) = \sum_{m=1}^{\infty} a_m R_0 \sin\{H_1(m)(\theta+\Delta\theta)\} + \sum_{l=1}^{\infty}\sum_{m=1}^{\infty} a_l a_m \left[\cos\left\{ H_2(l,m)(\theta - \frac{H_1(m)\Delta\theta}{H_2(l,m)}) \right\} - \cos\left\{ H_3(l,m)(\theta + \frac{H_1(m)\Delta\theta}{H_3(l,m)}) \right\} \right] \quad (5)$$

From (5), magnetic flux whose order is $H_1(m)$, $H_2(l,m)$, and $H_3(l,m)$ rotates with $\Delta\theta$, $-H_1(m)\Delta\theta/H_2(l,m)$, and $H_1(m)\Delta\theta/H_3(l,m)$, respectively. To operate as a reduction gear, the number of pole pairs in the low-speed rotor N_l should be equal to $H_2(l,m)$ or $H_3(l,m)$. Therefore, the relation among N_h, N_s, and N_l can be obtained as follows:

$$(2l-1)N_s = N_l \pm (2m-1)N_h \quad (6)$$

Then, the gear ratio G_r can be obtained as follows:

$$G_r = \mp \frac{(2m-1)N_h}{N_l} \quad (7)$$

III. Orders Contained in Cogging Torque

The cogging toque on the high-speed rotor $T(\theta)$ under the synchronous operation in accordance with the gear ratio is described in this section. $T(\theta)$ consists of the cogging torque generated by stationary pole pieces $T_1(\theta)$ and by the low-speed rotor $T_2(\theta)$.

According to the principle of the transformation from magnetic energy to mechanical energy, equation (8) can be obtained.

$$T(\theta) = -\frac{\partial W(\theta)}{\partial \theta} \quad (8)$$

where $W(\theta)$ is magnetic energy. Assuming that magnetic energy is stored only in the air gap, $W(\theta)$ is as follows:

$$W(\theta) = \frac{1}{2\mu_0}\int_V B^2 dV \quad (9)$$

where μ_0 is the permeability in vacuum, V is the volume of air gap, and B is magnetic flux density in the air gap.

The initial rotor angle of the high-speed rotor is represented θ=0, and the rotor angle δ is given to the high-speed rotor. Then, equation (9) is transformed to (11) with the volume difference of the air gap ΔV shown in (10).

$$\Delta V = L_s l_{g1}(2r_{g1}\pi \times \frac{d\delta}{2\pi}) = L_s l_{g1} r_{g1} d\delta \quad (10)$$

$$W(\theta) = \frac{L_s l_{g1} r_{g1}}{2\mu_0}\oint B^2 d\delta \quad (11)$$

where L_s is the axial length of the air gap, l_{g1} is the air-gap length between the high-speed rotor and the stationary pole pieces, and r_{g1} is the average air-gap radius.

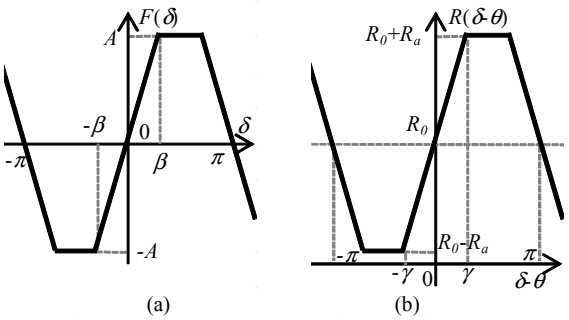

(a) (b)

Fig. 4 Distributions of (a) magnetomotive force and (b) permeance.

Magnetomotive force and permeance can be defined in Figs. 4(a) and 4(b) by employing δ.

Substituting magnetic flux density shown in (12) into (11) yields (13).

$$B = \frac{F(\delta)R(\delta-\theta)}{2r_{g1}L_s\pi} \quad (12)$$

$$W(\theta) = \frac{l_{g1}}{8\mu_0 r_{g1} L_s \pi^2}\int_0^{2\pi} F^2(\delta)R^2(\delta-\theta)d\delta \quad (13)$$

Fourier series expansions of $F^2(\delta)$ and $R^2(\delta-\theta)$ are shown in (14) and (15).

$$F^2(\delta) = a_{0F} + \sum_{n=1}^{\infty} a_n \cos 2nN_h\delta \quad (14)$$

$$R^2(\delta-\theta) = a_{0R} + \sum_{m=1}^{\infty} b_m \sin mN_s(\delta-\theta) \quad (15)$$

where a_{0F} and a_{0R} are constant.

Substituting (14) and (15) into the integral term of (13) yields (16).

$$F^2(\delta)R^2(\delta-\theta) = a_{0F}a_{0R} + \sum_{n=1}^{\infty} a_{0R}a_n \cos 2nN_h\delta + \sum_{m=1}^{\infty} a_{0F}b_m \sin mN_s(\delta-\theta) + \sum_{m=1}^{\infty}\sum_{n=1}^{\infty}\frac{a_n b_m}{2}\left[\sin\{(2nN_h+mN_s)\delta - mN_s\theta\} - \sin\{(2nN_h-mN_s)\delta + mN_s\theta\}\right] \quad (16)$$

where the first term in right-hand side of (16) becomes zero by the partial derivative by θ, the second, third, and fourth terms also become zero by the integral of δ. Therefore, the constraint that the cogging torque is generated must be that the fifth term is not zero. The cogging torque shown in (17) is obtained as equation (18) is satisfied.

$$T_1(\theta) = -\frac{\partial}{\partial\theta}\left\{\frac{l_{g1}}{8\mu_0 r_{g1}L_s\pi^2}\int_0^{2\pi}\sum_{m=1}^{\infty}\sum_{n=1}^{\infty} -\frac{a_n b_m}{2}\sin(mN_s\theta)\right\} \quad (17)$$

$$2nN_h - mN_s = 0 \quad (18)$$

The cogging torque on the high-speed rotor generated by the low speed-rotor $T_2(\theta)$ is given by the following procedure as well. N_l-$G_r N_l$ pole pairs in the low-speed rotor pass the high-speed rotor as the high-speed rotor makes a rotation. Therefore, assuming that the low-speed rotor is fixed, the number of pole pairs in the low-speed rotor can be regarded as N_l-$G_r N_l$. The magnetic field by the low-speed rotor is $G(\delta-\theta)$, and the magnetic field between two rotors $F(\delta)$+ $G(\delta-\theta)$, is shown as follows:

$$F(\delta)+G(\delta-\theta)=a_{0FG}+\sum_{n=1}^{\infty}c_n\cos nN_h\delta + \sum_{m=1}^{\infty}c_m\cos m(N_l-G_rN_l)(\delta-\theta) \tag{19}$$

where a_{0FG} is constant. The permeance between two rotors is constant, R_1. The integral term of (13) is represented as follows:

$$\begin{aligned}(F(\delta)+G(\delta-\theta))^2R_1^2 &= c_0^2R_1^2+\sum_{n=1}^{\infty}c_n^2R_1^2\cos^2 nN_h\delta \\ &+\sum_{m=1}^{\infty}c_m^2R_1^2\cos^2 m(N_l-G_rN_l)(\delta-\theta) \\ &+\sum_{n=1}^{\infty}2a_{0FG}c_nR_1^2\cos nN_h\delta \\ &+\sum_{m=1}^{\infty}2a_{0FG}c_mR_1^2\cos m(N_l-G_rN_l)(\delta-\theta) \\ &+\sum_{m=1}^{\infty}\sum_{n=1}^{\infty}2c_mc_nR_1^2\cos(nN_h\delta)\cos m(N_l-G_rN_l)(\delta-\theta)\end{aligned} \tag{20}$$

where only the sixth term generates cogging torque, and it is expanded as follows:

$$\sum_{m=1}^{\infty}\sum_{n=1}^{\infty}R_1^2c_mc_n[\cos[\{nN_h+m(N_l-G_rN_l)\}\delta-m(N_l-G_rN_l)\theta] + \cos[\{nN_h-m(N_l-G_rN_l)\}\delta+m(N_l-G_rN_l)\theta]] \tag{21}$$

Cogging torque is generated as equation (22) is satisfied. The cogging torque generated by the low-speed rotor $T_2(\theta)$ is represented in (23).

$$nN_h-m(N_l-G_rN_l)=0 \tag{22}$$

$$T_2(\theta)=-\frac{\partial}{\partial\theta}\left\{\frac{l_{g2}}{8\mu_0r_{g2}L_s\pi^2}\int_0^{2\pi}\sum_{m=1}^{\infty}\sum_{n=1}^{\infty}R_1^2c_mc_n\cos m(N_l-G_rN_l)\theta\right\} \tag{23}$$

where l_{g2} is the air-gap length between rotors, and r_{g2} is the average air-gap radius.

The cogging torque in the high-speed rotor $T(\theta)$ is represented as follows:

$$T(\theta)=-\frac{\partial}{\partial\theta}\left\{\frac{l_{g2}}{8\mu_0r_{g2}L_s\pi^2}\int_0^{2\pi}\sum_{m=1}^{\infty}\sum_{n=1}^{\infty}R_1^2c_mc_n\cos m(N_l-G_rN_l)\theta - \frac{l_{g1}}{8\mu_0r_{g1}L_s\pi^2}\int_0^{2\pi}\sum_{m=1}^{\infty}\sum_{n=1}^{\infty}\frac{a_nb_m}{2}\sin(mN_s\theta)\right\} \tag{24}$$

The cogging toque generated in the low-speed rotor can be obtained as well. Therefore, the order contained in cogging torque is summarized in Table I.

TABLE I
ORDERS CONTAINED IN COGGING TORQUE AND CONSTRAINTS

	Order Contained in Cogging Torque	Constraint
High-Speed Rotor	$m\,(N_l\text{-}G_rN_l)$	$nN_h=m\,(N_l\text{-}G_rN_l)$
	mN_s	$2nN_h=mN_s$
Low-Speed Rotor	$m\,(N_l\text{-}G_rN_l)$	$nN_h=m\,(N_l\text{-}G_rN_l)$
	mN_s	$2nN_l=mN_s$

IV. FINITE ELEMENT MODEL

A. Analysis Method

To verify the orders contained in cogging torque, 3-D FEM is employed. To solve the Maxwell's equation, the magnetic vector potential $\boldsymbol{A}$ is employed, and in this study, the eddy current is ignored. Then the fundamental equation is as follows:

$$\mathrm{rot}(\nu\,\mathrm{rot}\boldsymbol{A})=\nu_0\mathrm{rot}\boldsymbol{M} \tag{25}$$

where ν and ν_0 are the reluctivity of magnetic material and vacuum, respectively, $\boldsymbol{M}$ is the magnetization. Transmission torque is calculated by the nodal force method.

B. Analysis Model

The gear ratio of the analysis model is decided in accordance with (6). In this study, the specifications are shown in Table II, and the dimensions are shown in Table III. The analysis model is shown in Fig. 5. In this model, 14 pole pieces are connected by the flux path facing to the high-speed rotor, whose width is 0.5 mm, equal to the thickness of the laminated silicon steel sheet. This structure helps not only to assemble, but also reduce the cogging torque. However, it is thought that the maximum transmission torque slightly decreases due to the short-circuit magnetic flux.

V. TRANSMISSION TORQUE ANALYSIS

A. Analysis Condition

TABLE II
SPECIFICATIONS OF THE SPM-TYPE MAGNETIC GEAR IN THIS STUDY

Number of pole pairs in the high-speed rotor	4
Number of pole pairs in the low-speed rotor	10
Number of stationary pole pieces	14
Gear ratio	-2.5

TABLE III
DIMENSIONS OF THE SPM-TYPE MAGNETIC GEAR IN THIS STUDY

Outer radius of the high-speed rotor	R23
Inner radius of the stationary pole pieces	R24
Outer radius of the stationary pole pieces	R34
Inner radius of the low-speed rotor	R35
Outer radius of the low-speed rotor	R45
Axial length	26

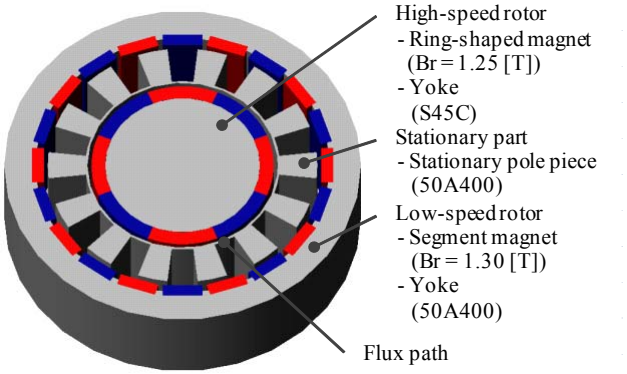

Fig. 5 Analysis model in this study.

The maximum transmission torque is generated as the phase difference between two rotors is 90 degrees. In this position, the constant rotation speed is given to both rotors in accordance with the gear ratio.

B. *Results of analysis*

The synchronous transmission torque was computed as shown in Fig. 6. The orders contained in the cogging torque on both rotors are shown in Figs. 7 and 8.

The cogging torque on the high-speed rotor and low-speed rotor is 0.013 Nm and 0.029 Nm, respectively, which are very small compared with its maximum transmission torque. This implies the flux path helps to reduce the cogging torque on the high-speed rotor.

The orders shown in Table I are found. The orders not shown there are the harmonic components (H.C.) by its pole pairs and stationary pole pieces. These orders appear because of the error of the mesh in the analysis model.

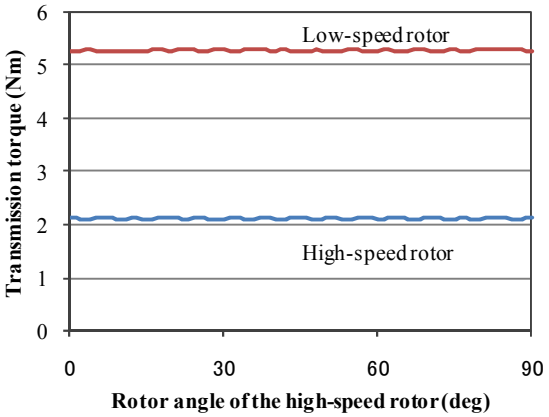

Fig. 6 Computed synchronous transmission torque.

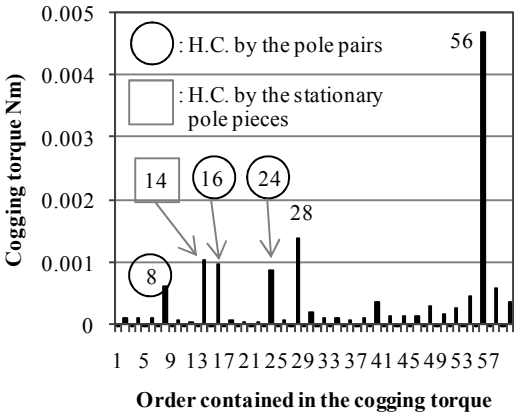

Fig. 7 Order contained in the cogging torque on the high-speed rotor.

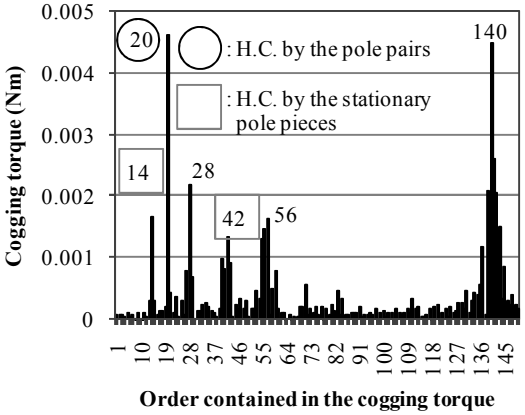

Fig. 8 Order contained in the cogging torque on the low-speed rotor.

VI. Verification by a Prototype

A. *Prototype and Torque Measuring System*

A prototype based on the specifications mentioned above was manufactured, and is shown in Fig. 9. This prototype is set to the torque measuring system shown in Fig. 10, and the constant rotation speed was given to both rotors in accordance with the gear ratio by the AC servo motors.

B. *Results of experiment*

A rotation speed of 0.5 rpm was given to the high-speed rotor to ignore the effect of the eddy current. The synchronous transmission torque shown in Fig. 11 was measured. The orders contained in the cogging torque on both rotors are shown in Figs. 12 and 13.

The cogging torque on the high-speed rotor and low-speed rotor is 0.064 Nm and 0.371 Nm, respectively, and higher than the computed values. This is because the measurement errors and the noise of the torque measuring

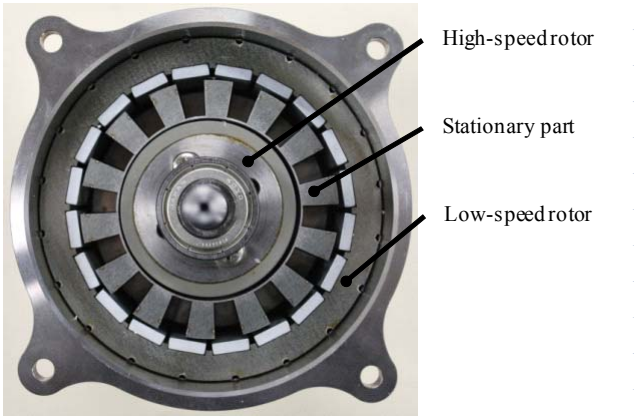

Fig. 9 Overview of the prototype magnetic gear.

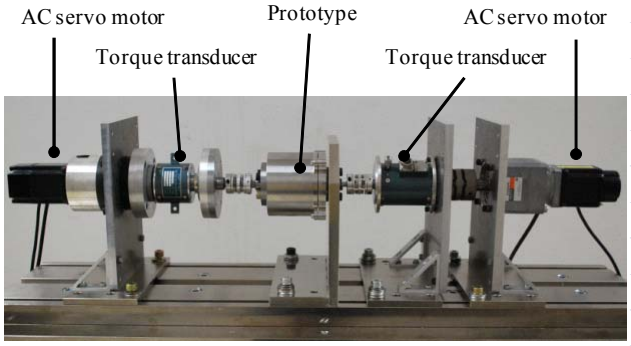

Fig. 10 Photograph of torque measuring system.

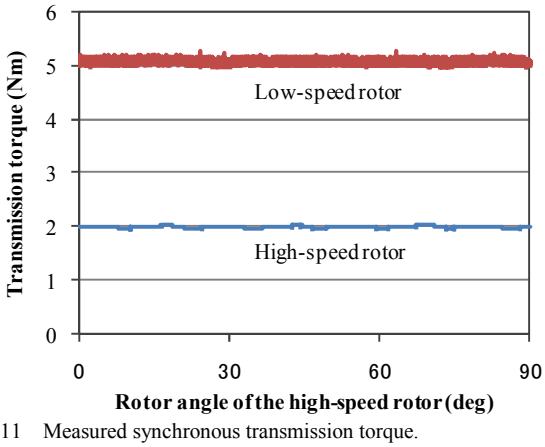

Fig. 11 Measured synchronous transmission torque.

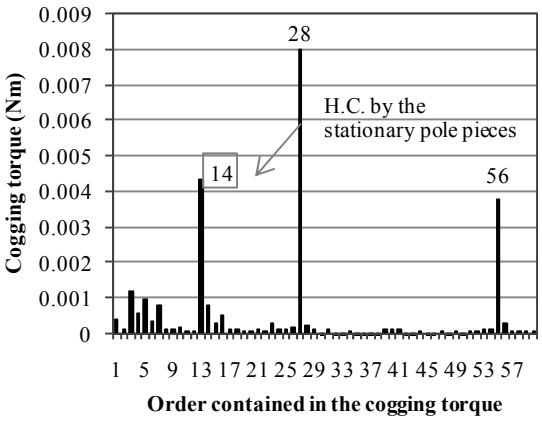

Fig. 12 Order contained in the cogging torque on the high-speed rotor.

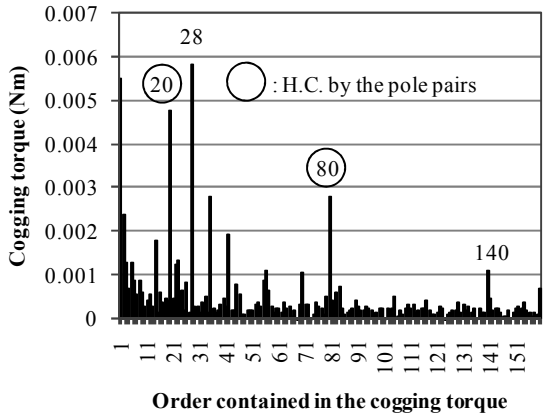

Fig. 13 Order contained in the cogging torque on the low-speed rotor.

system that is caused by the inverter of AC servo motors. The orders shown in Table I are found, whereas some harmonic components are contained. Thus, equation (24) shows the validity through the experiment.

VII. Cogging Torque Reduction

A. Finite Element Analysis of Skewed Model

The cogging torque against the maximum transmission torque on the high-speed rotor is higher than that on the low-speed rotor. Therefore, a step-skewed rotor which the number of steps is 2 is adopted in the high-speed rotor to reduce the cogging torque. And the 56th component predominates in the cogging torque on the high-speed rotor according to Fig. 7. Therefore, the phase difference between magnets is shifted with 3.2 degrees to reduce the 56th component.

The synchronous transmission torque shown in Fig. 14 was computed. The orders contained in the cogging torque on both rotors are shown in Figs. 15 and 16.

The cogging torque on the high-speed rotor and low-speed rotor is 0.012 Nm and 0.028 Nm, respectively, and was slightly reduced. Sufficient reduction was not realized because of the errors of the meshes.

B. Experiment with Step-Skewed Rotor

A step-skewed rotor of a prototype is shown in Fig. 17 together with non-skew rotor. The synchronous transmission torque was measured under the same condition as shown in Fig. 18. The orders contained in the cogging torque on both rotors are shown in Figs. 19 and 20.

The cogging torque on the high-speed rotor and low-speed rotor is 0.067 Nm and 0.292 Nm, respectively. The 56th component in the cogging torque on the high-speed rotor was reduced to half, and the effect of the step-skewed rotor on cogging torque reduction was verified. However, the total cogging torque on the high-speed rotor is nearly equal to the prototype without step-skew because of the measurement errors.

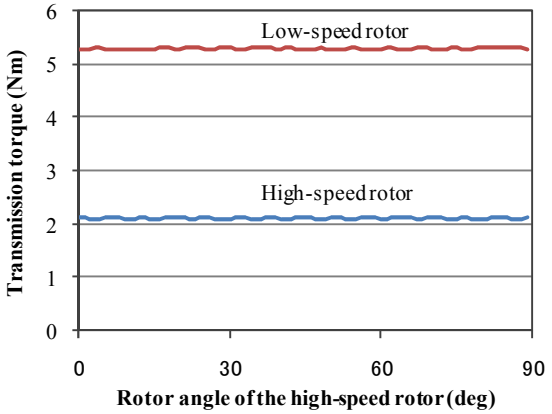

Fig. 14 Computed synchronous transmission torque.

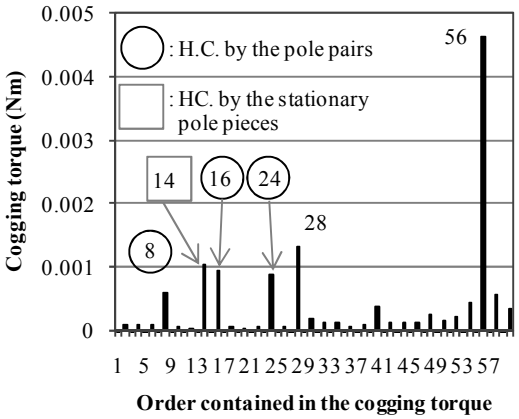

Fig. 15 Order contained in the cogging torque on the high-speed rotor.

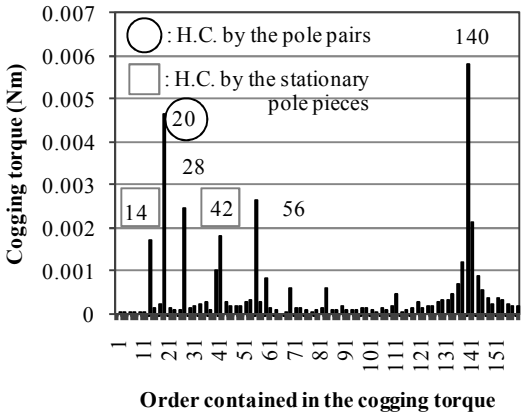

Fig. 16 Order contained in the cogging torque on the low-speed rotor.

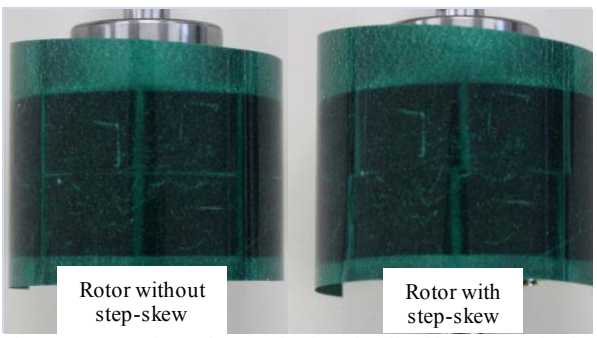

Fig. 17 Comparison of magnetization visualized by a magnetic viewer.

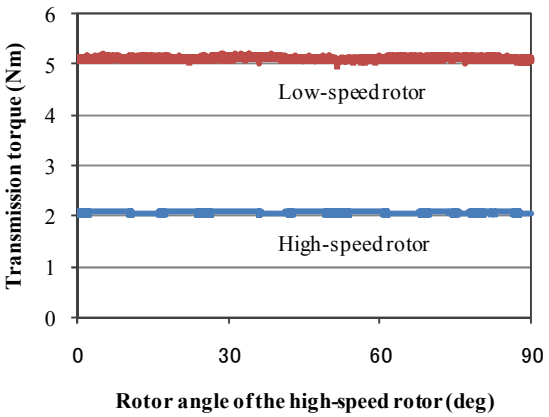

Fig. 18 Measured synchronous transmission torque.

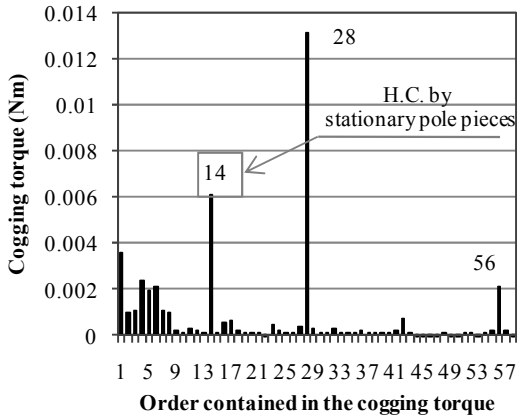

Fig. 19 Order contained in the cogging torque on the high-speed rotor.

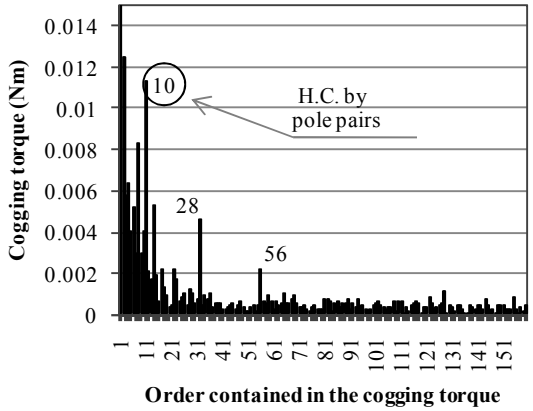

Fig. 20 Order contained in the cogging torque on the low-speed rotor.

The step-skewed rotor reduced the cogging torque on both rotors. But the low-order components contained in the cogging torque on the low-speed rotor stand out. This is because the noises in the torque measuring system influenced the measured value.

VIII. Conclusion

The operating principle and transmission torque characteristics in a SPM-type magnetic gear was formulated, and verified by employing the 3-D FEM analysis and the experiment. The cogging torque on the high-speed rotor is small enough against the maximum transmission torque. This is because the flux path mounted on the stationary pole pieces works well to reduce the cogging torque on the high-speed rotor.

The step-skewed rotor was proposed, but the sufficient reduction of the cogging torque was not obtained. In the near future, a new structure to reduce the cogging torque on both rotors will be proposed.

References

[1] P. O. Rasmussen, T. O. Andersen, F. T. Joergensen, and O. Nielsen, "Development of a High-Performance Magnetic Gear", *IEEE Trans. Industry Applications*, vol. 41, No. 3, pp. 764-770, May/June 2005.

[2] F. T. Joergensen, T. O. Andersen, and P. O. Rasmussen, "The Cycloid Permanent Magnetic Gear", *IEEE Trans. Industry Applications*, vol. 44, No. 6, pp. 1659-1665, Nov./Dec. 2008.

[3] J. Rens, R. Clark, S. Calverley, K. Atallah, and D. Howe, "Design, Analysis and Realization of a Novel Magnetic Harmonic Gear", in *Proc. International Conference on Electrical Machines* 2008.

[4] Jan Rens, Kais Atallah, Stuart D. Calverley, and David Howe, "A Novel Magnetic Harmonic Gear", *IEEE Trans. Industry Applications*, vol. 46, No. 1, pp. 206-212, Jan./Feb. 2010

[5] K. Atallah and D. Howe, "A novel high-performance magnetic gear", *IEEE Trans. Magn.*, vol. 37, No. 4, pp. 2844-2846, July 2001.

[6] R. Lateb, N. Takorabet, F. Meibody-Tabar, J. Enon, and A. Sarribouette, "Design technique for reducing the cogging torque in large surface mounted magnet motors", in *Proc. International Conference on Electrical Machines* 2004.

[7] K. Y. Lu, and P. O. Rasmussen, "An analytical equation for cogging torque calculation in surface mounted permanent magnet motors", in *Proc. International Conference on Electrical Machines* 2006.

[8] Bernard Laporte, "Cogging torque elimination in permanent magnet machines", in *Proc. International Conference on Electrical Machines* 2006.

[9] D, van Riesen, C. Schlensok, B. Schmulling, and K. Hameyer, "Cogging Torque Analysis on PMSM Machines by Simulation and Measurement", in *Proc. International Conference on Electrical Machines* 2006.

[10] M. Marinescu, N. Marinescu, and W. Wagner, "Reduction of the cogging torques of permanentmagnet excited motors with radial flux by the poleshifting method", in *Proc. International Conference on Electrical Machines* 2006.

[11] D. Lin, P. Zhou, and Z. J. Cendes, "Analytical Prediction of Cogging Torque in Spoke Type Permanent Magnet Motors", in *Proc. International Conference on Electrical Machines* 2008.

[12] Z. Q. Zhu, J. T. Chen, L. J. Wu, and D. Howe, "Influence of Stator Asymmetry on Cogging Torque of Permanent Magnet Brushless Machines", *IEEE Trans. Magn.*, vol. 44, No. 11, pp. 3851-3854, Nov. 2008.

Noboru Niguchi received the B.S. and M.S. degrees from Osaka University, Japan, in 1998 and 2000, respectively.

He is currently a student in the Department of Adaptive Machine Systems, Graduate School of Engineering, at Osaka University. He has been engaged in research of electrical machines. IEEE student member.

Katsuhiro Hirata received the B.E. degree from Osaka University in 1982 and D.E. degree from Doshisha University in 1996, respectively. He was a researcher at the R&D lab., Matsushita Electric Works Ltd. from 1982 to 2005. He jointed Osaka University in 2005. He is presently a professor in the Department of Adaptive Machine Systems, Graduate School of Engineering at Osaka University. He has been engaged in research of electromagnetic applied actuators and sensors. He has received Ministry Award of Education, Science & Technology (Ministry of Education, Culture, Sports, Science and Technology-Japan) in 2003. IEEE member. He has received OHM Technology Award (Promotion Foundation for Electrical Science and Engineering) in 2004. He received Advanced Technology Award and Paper Award (IEEJ) in 2007, 2009

Masari Muramatsu received the B.S. degree from Kanazawa University, Japan, in 2008.

He is currently a student in the Department of Adaptive Machine Systems, Graduate School of Engineering, at Osaka University. He has been engaged in research of electrical machines.

Yuichi Hayakawa received the B.S. degree from Osaka University, Japan, in 2009.

He is currently a student in the Department of Adaptive Machine Systems, Graduate School of Engineering, at Osaka University. He has been engaged in research of electrical machines.